CrossMark

REGULAR PAPER

M. Jadidi · V. Sreekumar · A. Dolatabadi

Breakup of elliptical liquid jets in gaseous crossflows at low Weber numbers

Abstract Breakup of circular and elliptical liquid jets in subsonic gaseous crossflows is experimentally studied using shadowgraph technique. The experiments are performed at gaseous Weber numbers less than 15, the liquid-to-gas momentum flux ratio between 50 and 320, and the orifice aspect ratio between 0.22 and 4.47. It is found that in addition to the momentum flux ratio, the orifice aspect ratio can change the liquid penetration height significantly. For a fixed momentum flux ratio, the penetration of elliptical jets is less than that of circular jet. Moreover, for a given momentum flux ratio and Weber number, the column breakup location of elliptical jets is earlier than that of circular jet. Empirical correlations for the penetration height as well as the column breakup location of circular and elliptical jets are developed in this study.

Keywords Breakup · Elliptical jet · Circular jet · Crossflow · Penetration height

1 Introduction

Injection of liquid jet in a gaseous crossflow is an important phenomenon which finds its application in fields like thermal spray coatings, spray drying, and combustion in a gas turbine engine, ramjet, or scramjet (Wu et al. 1997; No 2015; Jabbari et al. 2014; Jadidi et al. 2015, 2016; Wu et al. 2016). The liquid column deformation, surface waves, and primary breakup apparently control the spray characteristics such as penetration height, column breakup point (CBP), spray spread angle, and droplet size distribution (Sallam et al. 2004; Lee et al. 2007; Herrmann 2010; Song et al. 2011). Hence, it is necessary to study the near field behavior of transverse liquid jets in crossflows to improve the performance of these processes. In general, the spray produced by a liquid jet in crossflow is divided into three regions: intact liquid column, ligaments, and droplets. In the intact liquid column region, the surface waves grow along the jet column (windward surface) until the rupture occurs and small liquid segments, named ligaments, are formed. This phenomenon is referred to as the column breakup. Smaller droplets are formed by the further breakup of ligaments (which is known as secondary breakup). It is worth mentioning that for high values of liquid-to-gas momentum flux ratio and gaseous Weber number, the surface waves with short wavelengths grow on the lower (i.e., leeward) surface of the liquid jet. In this case, very small droplets are sheared off the leeward surface, which is called surface breakup. Clearly, one of the main parameters that might have significant effects on near field behavior and therefore on spray characteristics, is the geometry of liquid orifice.

The effect of orifice geometry on the breakup mechanisms of liquid jets in still air has been investigated in recent years (Bechtel et al. 1995; Kasyap et al. 2009; Amini and Dolatabadi 2012; Sharma and Fang 2014; Wang and Fang 2015). It was found that noncircular liquid jets may breakup earlier than circular jets.

M. Jadidi (✉) · V. Sreekumar · A. Dolatabadi
Department of Mechanical, Industrial and Aerospace Engineering, Concordia University, Montreal, QC H3G 1M8, Canada
E-mail: m_jadi@encs.concordia.ca

Among different noncircular nozzle configuration, the elliptical orifices have attracted many attentions. Elliptical liquid jets tend to configurations with minimum surface energy. As a result, several inherent instabilities such as axis-switching phenomenon cause these jets to breakup faster with less energy (Bechtel et al. 1995; Kasyap et al. 2009; Amini and Dolatabadi 2012).

The behavior of elliptical liquid jets in gaseous crossflows has not been studied comprehensively so far. Farvardin and Dolatabadi (2012) numerically studied the primary breakup of elliptical liquid jets in crossflows using volume of fluid model. They found significant changes in liquid column before disintegration for different aspect ratios. As a result, penetration height and droplet size distribution were affected by the orifice geometry and orientation. The aspect ratio (A_r) was defined in their study as the ratio of dimension of the orifice axis perpendicular to the air flow to the dimension of the orifice axis parallel to the air flow (shown in Fig. 1), in order to take the jet ellipticity and its orientation into account. Using the same definition of aspect ratio, Marzbali (2011) developed a theoretical model to estimate the trajectories of elliptical jets with various aspect ratios in crossflows. Based on his model, the elliptical jets with lower aspect ratios penetrate deeper into the crossflow. It is worth mentioning that, in his work, the effect of drag force on the jet trajectory is considered and other phenomena such as axis-switching, liquid turbulence, and mass shedding from jet surface were ignored. Morad and Khosrobeygi (2019) also experimentally studied the penetration of elliptical liquid jets in low-speed crossflow and proposed an empirical correlation for jet trajectory. However, the effect of orifice orientation on the primary breakup and liquid penetration height is not clear in their study, since the aspect ratio was defined as the ratio of the major to minor axis.

In the current work, an experimental study is performed to investigate the near field behavior of elliptical and circular liquid jets in low weber number crossflows (The Weber number in this study is less than 15.) In other words, the objective of this study is to gain a deeper understanding of the primary breakup phenomenon and to compare the behavior of elliptical jets against the circular jets. The shadowgraph images are used to visualize the breakup details. The effects of geometry such as variation in aspect ratio and orientation of elliptical nozzles are taken into consideration. Three parameters are of importance to our study: (1) the penetration height of liquid jet in crossflow, (2) the column breakup point location, and (3) bag onset location and length.

2 Experimental setup

The experimental test facility used in this study comprises of an open loop subsonic wind tunnel with a test section of $100 \times 100 \times 750$ mm, liquid injection system, and a high-speed camera. The test section is made of transparent acrylic material for visualization purposes. A schematic of the experimental setup is shown in Fig. 2. A 1.5-HP blower fan made by Aeroflo (Mississauga, Ontario, Canada) is used to blow the ambient air into the wind tunnel. After passing through a fine screen and a nozzle, the flow reaches the test section. The air velocity inside the test section is controlled using Honeywell Torque Control Adjustable Speed Drive and can be varied between 6.5 and 45 m/s. The air velocity in the test section was characterized by particle image velocimetry (PIV) measurements of a very fine spray, and the velocity vectors as well as turbulence intensity were reported in the work of Farvardin (2013). The PIV results showed that in the test section, the air velocity is parallel and constant except for the narrow boundary layers on the wall. The boundary layer thickness near the injector location is smaller than 10 mm which is much less than the liquid jet penetration height. Furthermore, the PIV measurements showed that at the test section just upstream of the injector location, a turbulence intensity of 9% exists. In the current study, the Pitot tube is used to measure the air velocity inside the test section.

The liquid injection system consists of a pressure vessel, a flowmeter, and different circular/elliptical test injectors. Distilled water is used as the test liquid throughout the experiment. The injectors have plain orifices with length to diameter of 10. Circular orifice with diameter of 0.43 mm and two elliptical orifices are machined on aluminum plates, using the electro discharge method. Area of elliptical orifices is the same as that of circular orifice and is equal to 0.145 mm^2. In other words, the equivalent diameter of different orifices is 0.43 mm. It should be noted that due to machining process, there were small differences in the cross-sectional area of the nozzles. However, the error is within 5% of the mentioned equivalent diameter. In this study, the aspect ratio (A_r) has the same definition as that provided in the works of Marzbali (2011) and Farvardin and Dolatabadi (2012) (see Fig. 1). Elliptical orifices of aspect ratios 0.224, 0.7, 1.43, and 4.47, and circular orifice of aspect ratio 1, are used in this study. Moreover, a tapered transition from the 2 to 0.43 mm is designed to avoid cavitation inside the orifice (Farvardin et al. 2013). Water jet velocities (i.e.,
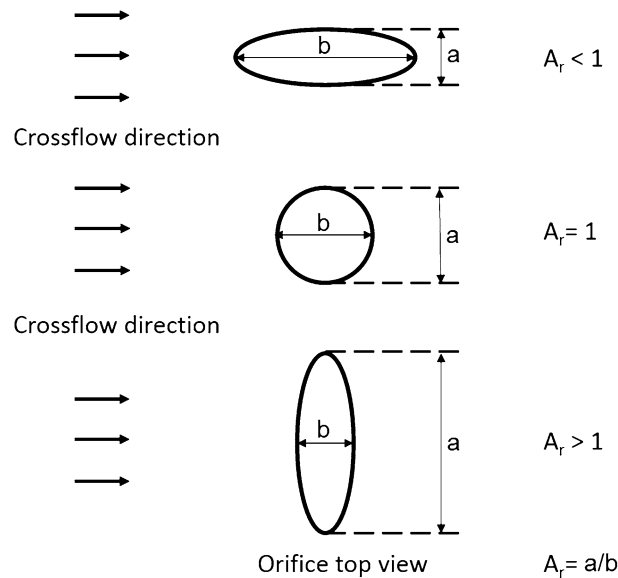
Fig. 1 Schematic representation of nozzle aspect ratio

water volume flow rate/orifice area) are varied from 2.3 to 18.7 m/s. The injectors are mounted flush with the upper wall of the test section at an axial position of 200 mm from its inlet plane. The orifices centers lie on the symmetry plane of the test section.

The Photron SA1.1 high-speed digital camera, set at 5000 frames per second with a resolution of 1024 × 1024 and a lens (AF Micro-Nikkor 105 mm f/2.8, Nikon), is used to record the side-view images of the breakup phenomenon and jet's trajectory. Two halogen lamps (type: T-3, 200T3Q/CL/78MM, Satco, USA) were used for backlighting. The data from these images are extracted using ImageJ and plot digitizer image processing software. For each of the testing conditions, the coordinates of the jet windward trajectory as well as the column breakup point (CBP) location and other parameters are obtained every 10 ms (or every 50 images) manually without applying any threshold criteria. These values are then averaged and presented in this study. It is worth mentioning that this approach is based on the works of Herrmann et al. (2011) and Lubarsky et al. (2012) and was also used in our previous paper (Jadidi et al. 2017). Herrmann et al. (2011) discussed that usually to determine the mean jet penetration and the CBP location, the side-view shadowgraphy images are either first averaged and then thresholded, or the individual images are first thresholded and then averaged. The threshold value applied in either case ranges anywhere from 3% of the
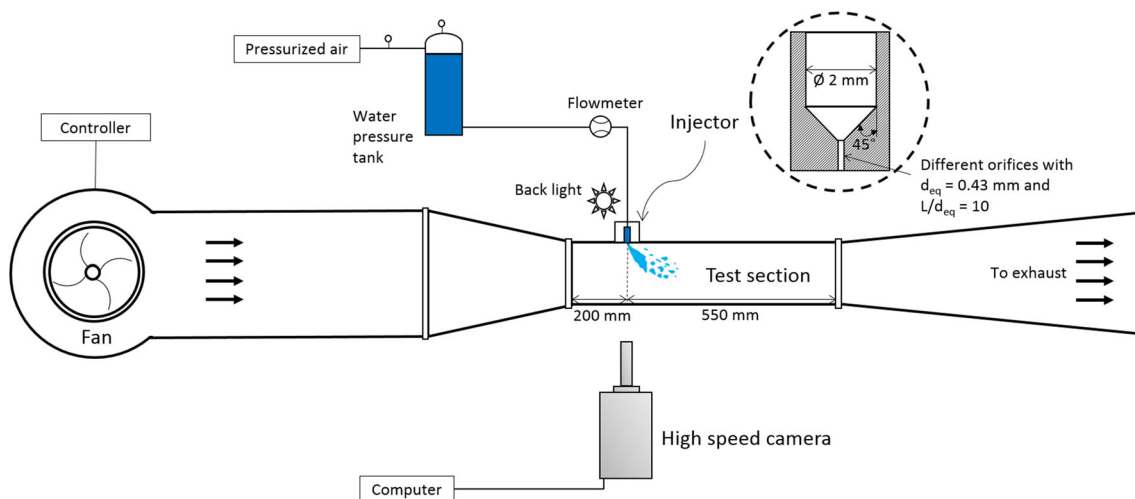

Fig. 2 A schematic of experimental setup and internal nozzle geometry

maximum image intensity to 50% of the local image line maximum intensity. However, their results showed that the value of threshold used to identify the leading edge has significant influence on the penetration correlations for the windward trajectory. In addition, Lubarsky et al. (2012) explained that the imaging technique and superposition of spray images on one image can be one of the main reasons why the spray trajectories available in the literature differ from each other significantly. In their work, the CBP position and other parameters were obtained from 150 images and the resulting values were then averaged. The same approach is followed in the current study. Experiments are conducted at atmospheric pressure and room temperature and are repeated four times for each momentum flux ratio, Weber number, and aspect ratio. Overall, more than 300 experiments are performed and more than 1.5 million images are saved.

3 Results and discussion

A low-speed water jet coming out of circular and elliptical nozzles under the absence of air crossflow is represented in Fig. 3. It can be observed that the jet exiting the circular nozzle undergoes a smooth flow without any considerable disturbances, while the jet from the elliptical nozzle experiences axis-switching multiple number of times (Bechtel et al. 1995; Kasyap et al. 2009; Amini and Dolatabadi 2012). The axis-switching phenomenon depends on factors such as aspect ratio, liquid Weber number, and turbulent intensity (i.e., nozzle geometry and internal design).

By increasing the crossflow velocity, the liquid jet bends toward the crossflow direction. In Fig. 4, the enhanced capillary breakup regime, which is observed at very low gaseous Weber number ($We = \rho_g U_g^2 d/\sigma$, where ρ_g, U_g, d, and σ are gas density, velocity, equivalent orifice diameter and surface tension, respectively) conditions, is shown. In this Figure, the effects of aspect ratio (A_r) and axis-switching on breakup mechanism, liquid penetration height, and breakup length are presented. It is shown that the existence of axis-switching in elliptical jets causes the breakup length to decrease significantly. It may be observed that in addition to liquid-to-gas momentum flux ratio ($q = \rho_l U_l^2/\rho_g U_g^2$, where ρ_l and U_l are liquid density and velocity, respectively), the aspect ratio has some effects on the liquid penetration height. The main reason can be due to dependency of aerodynamics (e.g., drag) forces on the jet projected area and therefore on the aspect ratio. Furthermore, the qualitative observation clearly reveals that for low liquid velocity (i.e., low liquid Reynolds number) cases, liquid turbulence effects are negligible and the liquid–gas interface is smooth without significant disturbances. On the other hand, Fig. 5 shows that the turbulence effects are more prominent with the increase in the liquid velocity (i.e., increase in the liquid Reynolds number) and can even diminish the axis-switching phenomenon. It should be pointed out that in identical operating conditions, circular nozzle ($A_r = 1$) shows much lesser signs of turbulence. Figure 5 also reveals that for very low and very high aspect ratios (i.e., $A_r = 0.22$ and 4.47), the axis-switching is strong enough to compete with the effects of turbulence, and consequently, axis-switching with strong disturbances on the interface is visible. Indeed, the breakup phenomenon strongly depends on three parameters: axis-switching, aerodynamic forces, and liquid turbulence.

Generally, in addition to the liquid Reynolds number, the liquid structure at the nozzle exit depends on the length/diameter ratio of the injector nozzle (L/d), nozzle internal design (sharp edge or round edge orifices), surface roughness, and nozzle geometry. Regarding the effect of the length/diameter (L/d) ratio of the injector nozzle on the liquid structure near the nozzle exit as well as the jet penetration and droplet size, Surya Prakash et al. (2018) used various circular nozzles and performed several experiments under the absence of air crossflow. They showed that for liquid Reynolds number of 2545 and L/d of 10, the liquid jet appears smooth near the nozzle exit. However, for the same liquid Reynolds number, injectors with L/d of 50 and 100 demonstrated a higher degree of instability (i.e., significant disturbances on the liquid surface) when compared to L/d of 10. Furthermore, a similar behavior was observed with an increase in the liquid Reynolds number from the same injector. For a liquid Reynolds number of 5090, they also showed that the jet from the nozzle having an L/d of 10 appears smooth near the nozzle exit; however, the jet from the nozzle with L/d of 100 displays instability right from the nozzle exit. For a circular orifice, similar results are obtained in the current study. Lubarsky et al. (2012), Broumand et al. (2017), and Broumand and Birouk (2017) studied the effect of nozzle internal design on the liquid structure near the nozzle exit and liquid penetration height. In the work of Lubarsky et al. (2012), two different injectors, one injector with a sharp edge and another one with a round edge (i.e., smooth transition path from the plenum to the orifice) were investigated. They showed that, for the same liquid Reynolds number and without cross airflow, the jet injected from a sharp edge orifice expands and forms spray structures, ligaments, and droplets, while the jet
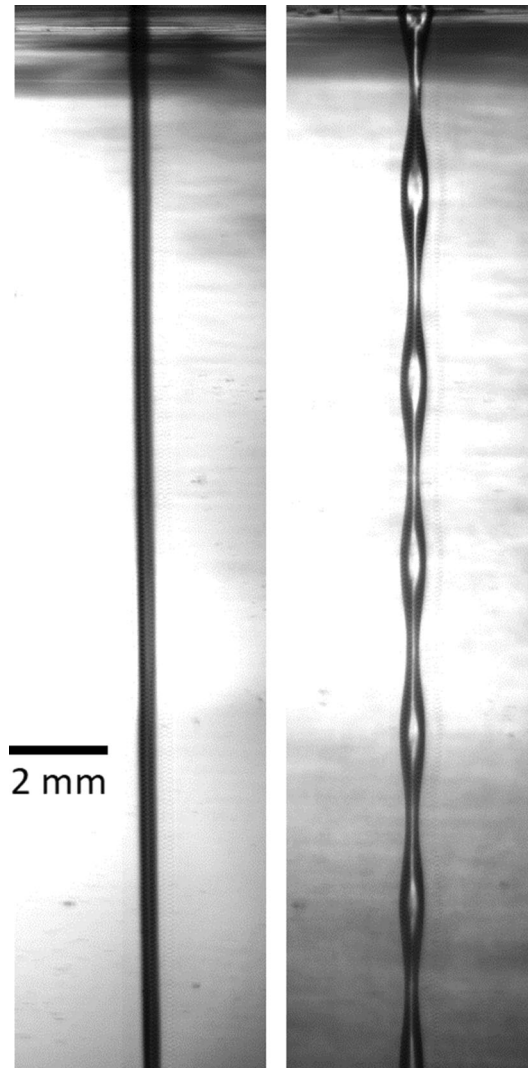
Fig. 3 Water jet from circular nozzle vs elliptical nozzle under the absence of a crossflow; liquid Reynolds number (Re_l, based on the equivalent diameter) is 1115

injected from the round edge nozzle displayed the development of the hydrodynamics instabilities and was relatively smooth and intact near the nozzle exit. Regarding the nozzle geometry and ellipticity, Ku et al. (2011) and Yu et al. (2018) investigated the effect of internal flow structure in circular and elliptical nozzles on spray characteristics under high injection pressure. Ku et al. (2011) found that, at the same injection pressure, the jet injected from the elliptical nozzle becomes more unstable compared to that of circular nozzle since the internal flow structure of the elliptical nozzle is significantly different. Yu et al. (2018) revealed that the vorticity magnitudes at the elliptical orifice exit are higher than that of the circular nozzle at the same injection pressure. They showed that, compared to the circular orifice, there are more turbulence vortex structures near the elliptical orifice exit. In addition, as the injection pressure increases, the number of turbulence vortex structures increases. It was concluded that the higher vorticity magnitude and more turbulence vortex structures at the elliptical nozzle exit can noticeably affect the liquid jet breakup as well as the spray penetration. Similar results can be observed in the current study as well. They also reported that at typical diesel engine conditions, the elliptical jet still exhibits axis-switching. In short, the significantly different behavior of elliptical jets, shown in Fig. 5, can be due to the effects of the surface roughness and internal flow structure of the elliptical nozzles.

As the gaseous Weber number increases to around 5, the bag breakup mechanism becomes dominant (Sallam et al. 2004; Jadidi et al. 2016). The liquid jet undergoes a particular length of deformation before
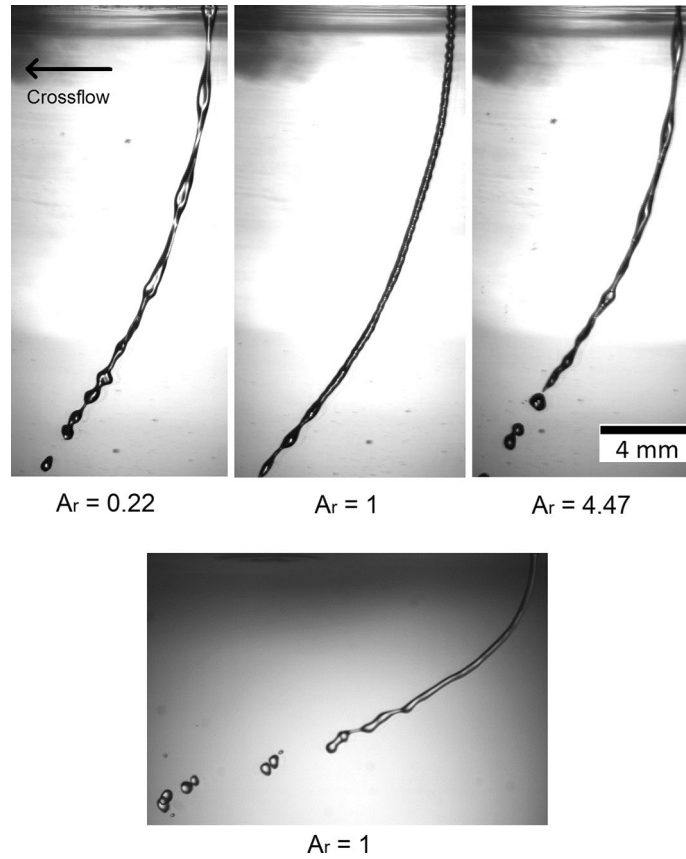
Fig. 4 Enhanced capillary breakup of elliptical jets vs circular jets; in the images at the top, liquid Reynolds number (Re_1), gaseous Weber number (We), and momentum flux ratio (q) are 2170, 1.6, and 76, respectively. In the images at the bottom, $Re_1 = 1115$, $We = 1.3$ and $q = 25$
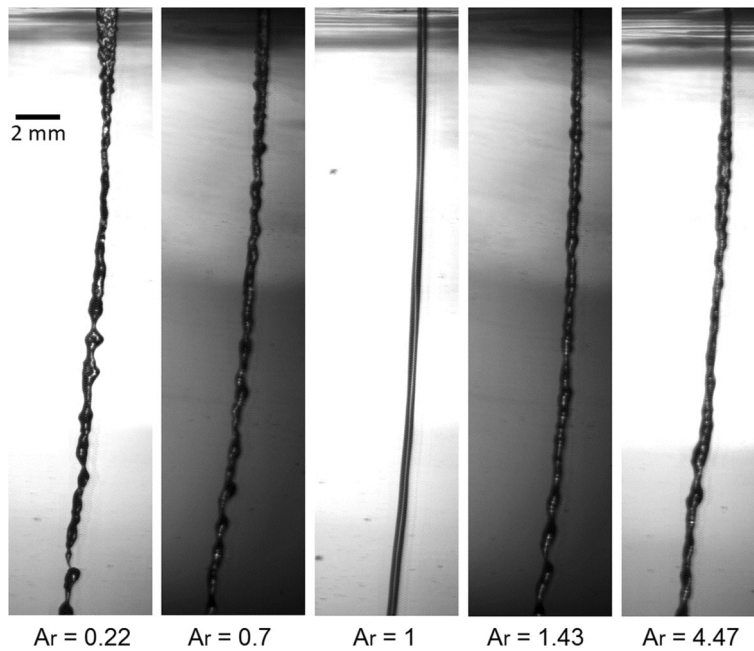

Fig. 5 Liquid turbulence at nozzle exit and its effects on axis-switching; $Re_1 = 5785$, $We = 1.6$ and $q = 540$

bag formation occurs on them as shown in Fig. 6 (Ng et al. 2008; Wang et al. 2012). This distance is called bag onset length denoted by L_{op}, and the cross-stream distance at which bag formation occurs is given by x_{op} (see Fig. 6). After bag formation, since the pressure inside the bag is greater than the pressure outside, the bag starts thinning and eventually it breaks when the surface tension is no longer enough to keep up with the aerodynamic force. As shown in Fig. 6, at the column breakup point (CBP) location (x_{cbp}, y_{cbp}), the liquid column ceases to exist and disintegrates into ligaments and droplets (Wang et al. 2012). In addition, the jet trajectory or the liquid penetration height is normally defined as the path taken by the lower boundary of the liquid jet (Wu et al. 1997; No 2015). The experimental observations on the jet trajectory, bag onset length, and CBP location prove that they are dependent on aspect ratio, gaseous Weber number, and momentum flux ratio or liquid Weber number [In other words, they depend on the aerodynamic forces, liquid turbulence, and the axis-switching that might happen before bag formation (see Figs. 7, 8, and 9)].

To show the effects of aerodynamic forces and liquid turbulence on the breakup mechanism, the behaviors of nonturbulent and turbulent circular liquid jets in gaseous crossflows, which were studied over the past decades, can be described here. For nonturbulent circular liquid jets in crossflows, the breakup mechanism depends on the aerodynamic forces (Li and Soteriou 2016). By increasing the gaseous Weber number, different breakup regimes such as bag, multimode, shear, and surface breakup can be observed (Wu et al. 1997; Sallam et al. 2004). Regular waves are detected on the liquid jet surface, and it is revealed that the wavelength decreases as the gaseous Weber number increases (Sallam et al. 2004; Xiao et al. 2013). On the other hand, it is shown that if the liquid jet is highly turbulent, bag and multimode breakup regimes are not observed at low Weber numbers (Lee et al. 2007). Moreover, the column breakup distance for the turbulent liquid jet is smaller than that for the nonturbulent liquid jet (Lee et al. 2007). It is also revealed that the liquid turbulence rather than the gaseous turbulence determines the jet instabilities and interface characteristics (Xiao et al. 2013). However, for elliptical liquid jets, the breakup phenomenon is more complicated due to the presence of axis-switching. The aerodynamic forces depend on the axis-switching and can vary significantly along the jet direction due to the liquid projected area changes. In addition, the liquid turbulence significantly affects the axis-switching and therefore the aerodynamic forces.

An empirical correlation for estimating the liquid penetration height or jet windward trajectory is developed in this study. As mentioned above, for each of the experimental conditions, the coordinates of jet windward trajectory were obtained at the interval of every 10 ms. The best-fit curves shown in Fig. 10 were obtained from these data using the curve fitting tool in MATLAB. The maximum root-mean-square error was obtained from $A_r = 4.47$ and was equal to 4.14 (see the bottom image in Fig. 10). The jet penetration height is normalized by the equivalent nozzle diameter and plotted against xq/d. It should be pointed out here that the quantitative results are only obtained from the cases with We greater than 5, where the bag breakup regime exists. As it can be observed, the jet trajectory depends on the liquid-to-gas momentum flux ratio and the aspect ratio. Like other works in this field (e.g., Wu et al. 1997; Masuda et al. 2005; Song et al. 2011; Lubarsky et al. 2012; Jadidi et al. 2016), it is found that the effect of gaseous Weber number on jet trajectory is negligible. It is clearly revealed that by increasing the momentum flux ratio, the jet penetration increases significantly. Furthermore, Fig. 10 shows that for a given momentum flux ratio, the jet penetration is the highest for circular nozzle ($A_r = 1$), followed by $A_r = 0.22$ and it is the least when $A_r = 4.47$. To explain why elliptical jets penetrate less compared to circular jets, two points should be considered: (1) In comparison with circular jet, the column breakup lengths in elliptical jets are smaller and the droplets/ligaments are formed earlier. Clearly, the acceleration rate of droplets/ligaments in crossflow direction is much higher than that of intact liquid column. Hence, the lower penetration heights in elliptical jets seem reasonable. (2) Drag force, which is the main parameter that controls the jet trajectory, depends on the aspect ratio and the axis-switching presence. When the minor axis of elliptical nozzle is aligned in the crossflow direction (e.g., $A_r = 4.47$), the effect of drag force becomes more important and significant reduction in jet penetration occurs. The recommended jet trajectory correlation for all the elliptical and circular jets is as follows:

$$\frac{y}{d} = \left(3.276 - 0.115A_r - 1.79A_r^{-0.05}\right)\left(\frac{xq}{d}\right)^{0.5} \tag{1}$$

It should be pointed out that for cylindrical nozzle ($A_r = 1$) the above equation changes to Wu's semiempirical correlation (1997).

In Fig. 11, the bag onset length (L_{op}) as well as x_{op} and column breakup point location (x_{cbp}, y_{cbp}) are presented for different aspect ratios (A_r), momentum flux ratios (q), and gaseous Weber numbers (We). For each test case, we extracted these data every 10 ms using the ImageJ software (i.e., the same procedure
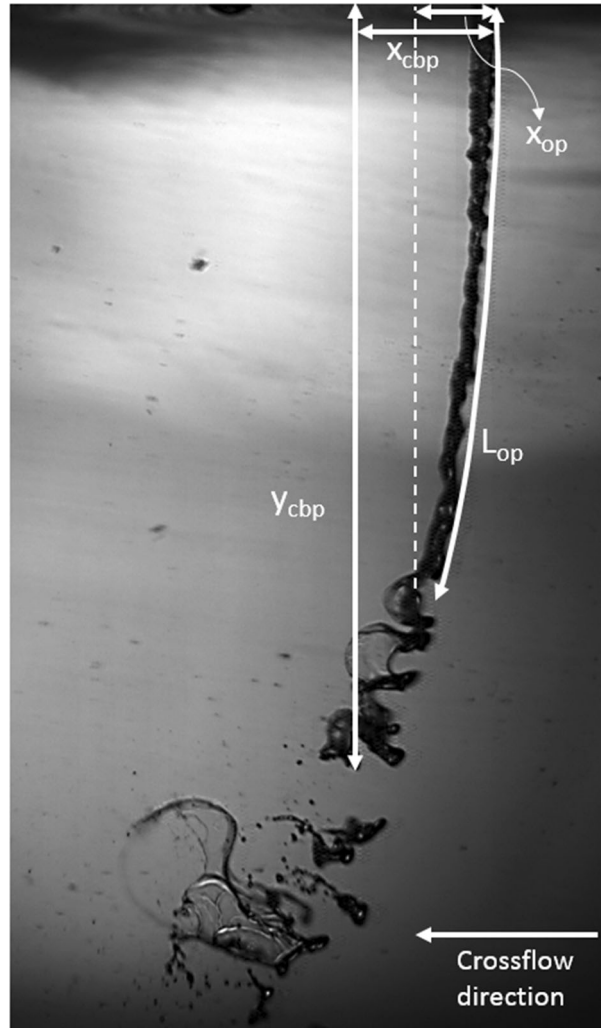
Fig. 6 Illustration of column breakup point location (x_{cbp}, y_{cbp}), bag onset length (L_{op}), and bag onset distance in crossflow direction (x_{op})

mentioned above) and then averaged. It is clear that as momentum flux ratio (q) increases, the bag onset length increases. On the other hand, the bag onset length depends inversely on the crossflow Weber number. It should also be noted that at a specific q and We, bag onset length is highest for circular nozzle ($A_r = 1$). The different liquid structures at the nozzle exit, shown in Fig. 5, can be the main reason why $A_r = 1$ shows very different results, and there is no continuity in the trend. As illustrated in Fig. 5, for the circular nozzle, the jet interface is smooth without significant disturbances. However, for elliptical nozzles, turbulent liquid jets exist. To show the effect of liquid turbulence on the bag formation, the behavior of turbulent and nonturbulent circular liquid jets in crossflow, studied by Wang et al. (2012), Ng et al. (2008), and Mazallon et al. (1998), can be compared. Wang et al. (2012) revealed that if the liquid jet is turbulent, the critical gaseous Weber number for bag formation will be considerably reduced. In addition, in identical operation conditions, the comparison between the works of Wang et al. (2012) and Ng et al. (2008) verifies that the onset length of bags in the case of turbulent liquid jet is less than that of nonturbulent liquid jet. It should also be noted that, change in the projected area along the jet direction for elliptical nozzles due to axis-switching can affect the active aerodynamic force, and therefore the bag onset length, significantly. Figure 11 also reveals that for elliptical nozzles ($A_r \neq 1$) at $We = 6.5$, increasing A_r causes L_{op} to increase slightly. However, for these nozzles ($A_r \neq 1$) at $We = 14.5$, increasing A_r results in a reduction of L_{op}. It is clear that as the crossflow Weber number or velocity increases, the effects of aerodynamic force and axis-switching on the breakup mechanism increase and decrease, respectively.
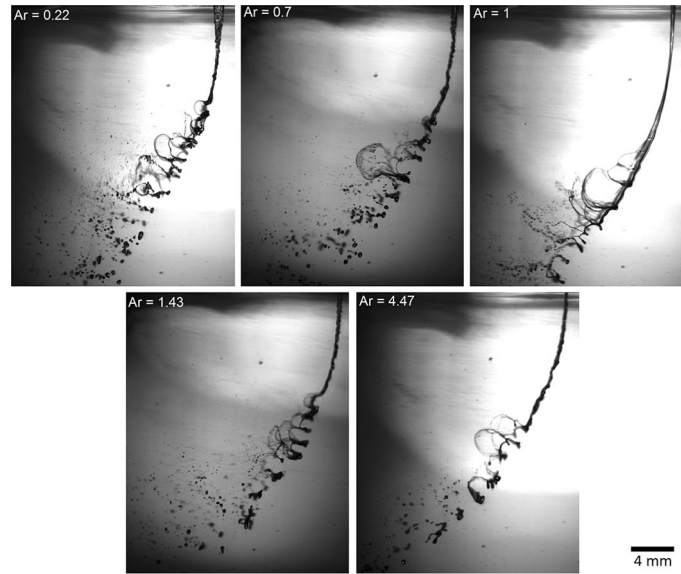
Fig. 7 Illustration of jet trajectory, bag formation and break up phenomena at different aspect ratio; $We = 6.5$ and $q = 126$
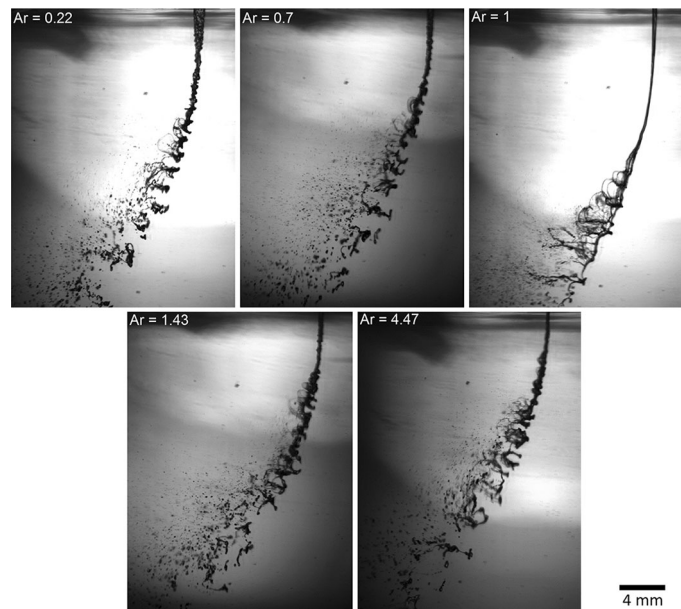

Fig. 8 Illustration of jet trajectory, bag formation and break up phenomena at different aspect ratio; $We = 14.5$ and $q = 141$

Figure 11 shows that for comparable values of momentum flux ratio ($q = 126$ vs. 141), x_{op} increases with decrease of We. Furthermore, for a constant We, decreasing q results in an increase of x_{op}. Like L_{op}, for elliptical nozzles ($A_r \neq 1$) at $We = 6.5$ and 14.5, increasing A_r causes x_{op} to increase and decrease, respectively. As shown, for $A_r = 4.47$, x_{op} changes significantly with We and q and can even be greater than that of circular jet. However, it is worth noting that the jet penetration in the case of $A_r = 4.47$ is much less compared to jet penetration in the cylindrical orifice case, and therefore, if L_{op} in these cases is similar, x_{op} for $A_r = 4.47$ should be greater.

The variations of column breakup location (x_{cbp}, y_{cbp}) with A_r, We, and q are also shown in Fig. 11. For a given value of Weber number, x_{cbp} is lower for higher value of momentum flux ratio. Moreover, for comparable values of momentum flux ratio, increasing the Weber number results in a reduction of x_{cbp}, which is in consistent with the numerical simulations of Li and Soteriou (2016) and Jadidi et al. (2017). For
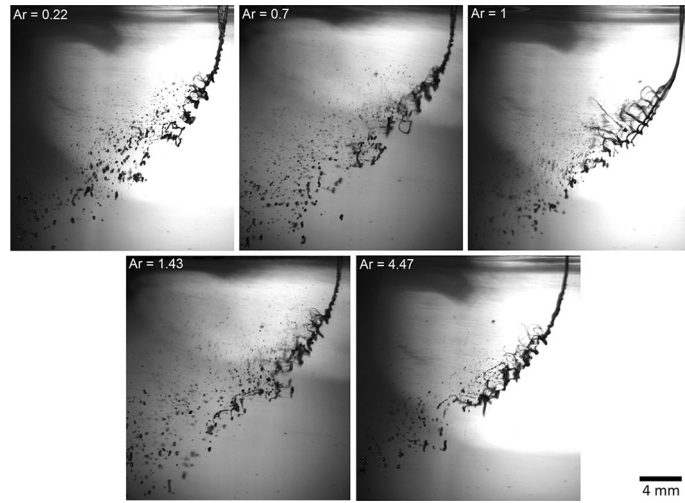
Fig. 9 Illustration of jet trajectory, bag formation and break up phenomena at different aspect ratio; *We* = 14.5 and *q* = 56
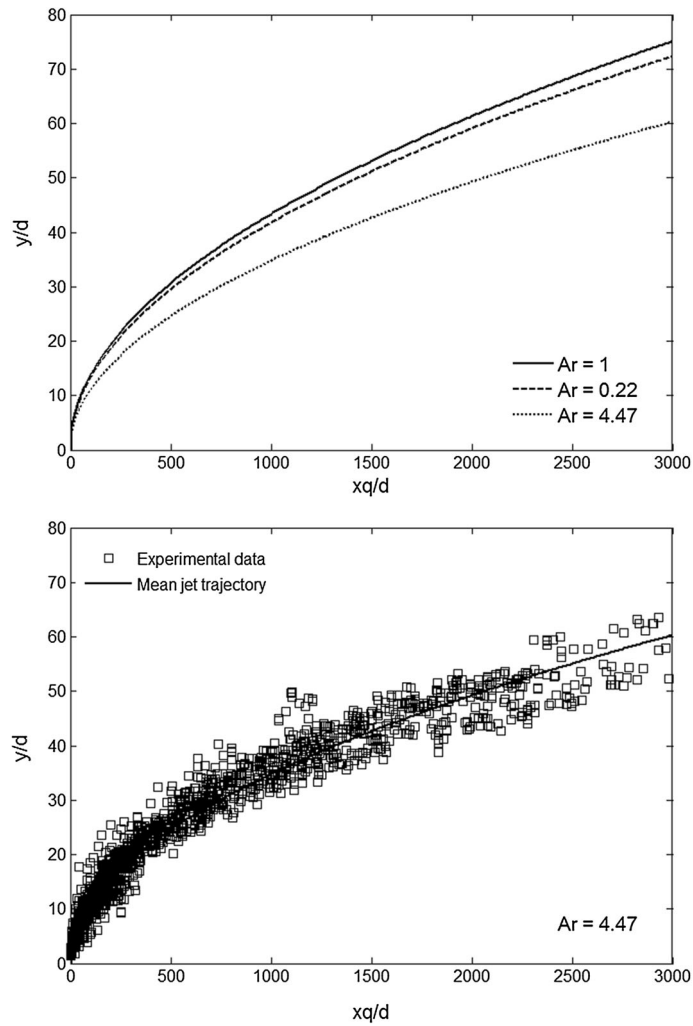

Fig. 10 Top image: mean jet trajectory as a function of aspect ratio (A_r) and momentum flux ratio (*q*); bottom image: mean jet trajectory with experimental data for A_r = 4.47; *d* is the equivalent diameter
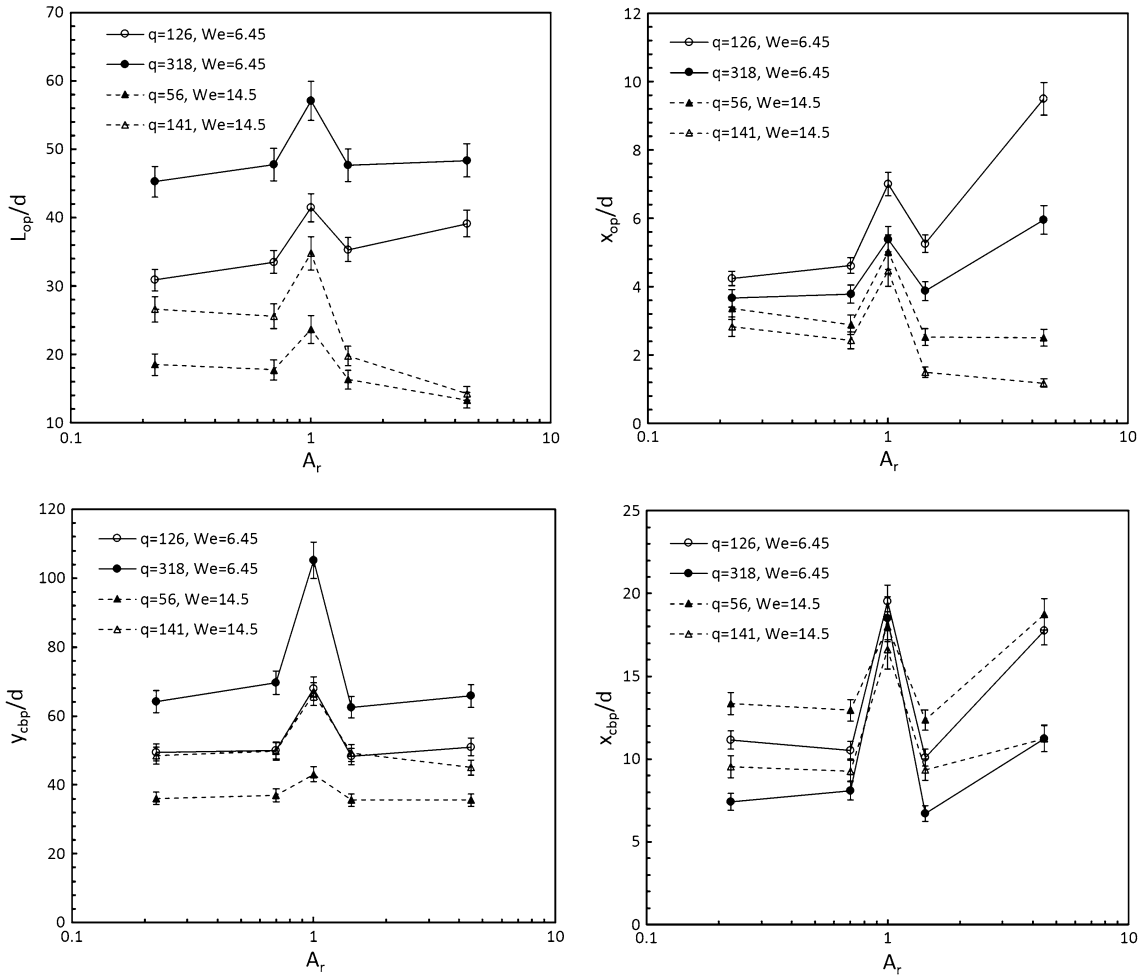
Fig. 11 The bag onset length (L_{op}), the cross-stream distance at which bag formation initiates x_{op}, and the liquid column breakup location (x_{cbp}, y_{cbp}) for different aspect ratios (A_r), momentum flux ratios (q), and gaseous Weber numbers (We)

a given We and q, the circular nozzle ($A_r = 1$) exhibits the highest values of x_{cbp}. However, for elliptical nozzles ($A_r \neq 1$), x_{cbp} is insensitive to changes in aspect ratio till $A_r = 1.43$. Higher aspect ratio (i.e., $A_r = 4.47$) leads to higher x_{cbp} values, due to lower jet penetration. On the contrary, y_{cbp} increases with increase in momentum flux ratio and it is not strongly sensitive to We (It can be claimed that the effect of Weber number on y_{cbp} at $A_r = 4.47$ is not negligible. However, the error would be less than 7% if we use the average y_{cbp}). It may be observed that for a given We and q, the circular nozzle ($A_r = 1$) has the highest y_{cbp}. However, y_{cbp} remains almost constant for other elliptical nozzles (i.e., $A_r \neq 1$). In general, the following correlations are recommended for estimating the column breakup location of circular and elliptical jets in gaseous crossflows:

$$\text{for } A_r = 1 \Rightarrow \quad \frac{y_{cbp}}{d} = 5.83q^{0.5}, \quad \frac{x_{cbp}}{d} = 18 \pm 1.5 \tag{2}$$

$$\text{for } A_r \neq 1 \Rightarrow \frac{y_{cbp}}{d} = 9.28q^{0.34}, \quad \frac{x_{cbp}}{d} = 134.63q^{-0.36}We^{-0.12}\left(3.276 - 0.115A_r - 1.79A_r^{-0.05}\right)^{-2} \tag{3}$$

4 Conclusion

Breakup of elliptical liquid jets in gaseous crossflows at low Weber numbers is experimentally investigated. Various elliptical orifices with the same area and equivalent diameter are used. It is found that the flow structures at the exit of circular and elliptical nozzles are significantly different. In identical operating conditions, the elliptical nozzles show more prominent signs of turbulence. It is also observed that the liquid

penetration height is a function of the orifice aspect ratio and the momentum flux ratio. For a given momentum flux ratio, the elliptical liquid jets penetrate less into the crossflows, compared to the circular jets. It is perhaps due to the effects of drag force and axis-switching. Furthermore, for a fixed momentum flux ratio and Weber number, the elliptical jets disintegrate earlier, most probably owing to liquid turbulence at the nozzle exit. Empirical correlations for the column breakup point location as well as the penetration height of circular and elliptical jets are developed.

References

Amini G, Dolatabadi A (2012) Axis-switching and breakup of low-speed elliptic liquid jets. Int J Multiph Flow 42:96–103

Bechtel SE, Cooper JA, Forest MG, Petersson NA, Reichard DL, Saleh A, Venkataramanan V (1995) A new model to determine dynamic surface tension and elongational viscosity using oscillating jet measurements. J Fluid Mech 293:379–403

Broumand M, Birouk M (2017) Effect of nozzle-exit conditions on the near-field characteristics of a transverse liquid jet in a subsonic uniform cross airflow. Phys Fluids 29:113303

Broumand M, Rigby G, Birouk M (2017) Effect of nozzle exit turbulence on the column trajectory and breakup location of a transverse liquid jet in a gaseous flow. Flow Turbul Combust 99:153–171

Farvardin E (2013) Biodiesel spray characterization: a combined numerical and experimental analysis. PhD Thesis, Concordia University, Montreal, Canada

Farvardin E, Dolatabadi A (2012) Breakup simulation of elliptical liquid jet in gaseous crossflow. In: AIAA 2012–2817

Farvardin E, Johnson M, Alaee H, Martinez A, Dolatabadi A (2013) Comparative study of biodiesel and diesel jets in gaseous crossflow. J Propuls Power 29(6):1292–1302

Herrmann M (2010) Detailed numerical simulations of the primary atomization of a turbulent liquid jet in crossflow. J Eng Gas Turbines Power 132:061506

Herrmann M, Arienti M, Soteriou M (2011) The impact of density ratio on the liquid core dynamics of a turbulent liquid jet injected into a crossflow. J Eng Gas Turbines Power 133:061501

Jabbari F, Jadidi M, Wuthrich R, Dolatabadi A (2014) A numerical study of suspension injection in plasma spraying process. J Therm Spray Technol 23:3–13

Jadidi M, Moghtadernejad S, Dolatabadi A (2015) A comprehensive review on fluid dynamics and transport of suspension/liquid droplets and particles in high-velocity oxygen-fuel (HVOF) thermal spray. Coatings 5(4):576–645. https://doi.org/10.3390/coatings5040576

Jadidi M, Moghtadernejad S, Dolatabadi A (2016) Penetration and breakup of liquid jet in transverse free air jet with application in suspension-solution thermal sprays. Mater Des 110:425–435

Jadidi M, Moghtadernejad S, Dolatabadi A (2017) Numerical simulation of primary breakup of round nonturbulent liquid jets in shear-laden gaseous crossflow. At Sprays 27(3):227–250

Kasyap TV, Sivakumar D, Raghunandan BN (2009) Flow and breakup characteristics of elliptical liquid jets. Int J Multiph Flow 35:8–19

Ku KW, Hong JG, Lee CW (2011) Effect of internal flow structure in circular and elliptical nozzles on spray characteristics. At Sprays 21:655–672

Lee K, Aalburg C, Diez F, Faeth GM, Sallam KA (2007) Primary breakup of turbulent round liquid jets in uniform crossflows. AIAA J 45(8):1907–1916

Li X, Soteriou MC (2016) High fidelity simulation and analysis of liquid jet atomization in a gaseous crossflow at intermediate Weber numbers. Phys Fluids 28:082101

Lubarsky E, Shcherbik D, Bibik O, Gopala Y, Zinn BT (2012) Fuel jet in cross flow—experimental study of spray characteristics. In: Oh HW (ed) Advanced fluid dynamics. InTech. https://doi.org/10.5772/26045

Marzbali M (2011) Penetration of circular and elliptical liquid jets into gaseous crossflow: a combined theoretical and numerical study. MS Thesis, Concordia University, Montreal, Canada

Masuda BJ, Hack RL, McDonell VG, Oskam GK, Cramb DJ (2005) Some observations of liquid jets in crossflow. In: Proceedings of the 18th annual conference on liquid atomization and spray systems, ILASS Americas, Irvine, California, USA, 22–25 May 2005

Mazallon J, Dai Z, Faeth GM (1998) Aerodynamics primary breakup at the surface of nonturbulent round liquid jets in crossflow. In: Proceedings of the 36th aerospace sciences meeting and exhibit, AIAA, Reno, Nevada, USA, 12–15 January 1998

Morad MR, Khosrobeygi H (2019) Penetration of elliptical liquid jets in low-speed crossflow. J Fluids Eng 141:011301

Ng CL, Sankarakrishnan R, Sallam KA (2008) Bag breakup of nonturbulent liquid jets in crossflow. Int J Multiph Flow 34(3):241–259

No SY (2015) A review on empirical correlations for jet/spray trajectory of liquid jet in uniform cross flow. Int J Spray Combust Dyn 7:283–314

Sallam KA, Aalburg C, Faeth GM (2004) Breakup of round nonturbulent liquid jets in gaseous crossflow. AIAA J 42(12):2529–2540

Sharma P, Fang T (2014) Breakup of liquid jets from non-circular orifices. Exp Fluid 55:1666

Song J, Ahn K, Kim MK, Yoon Y (2011) Effects of orifice internal flow on liquid jets in subsonic crossflows. J Propuls Power 27(3):608–619

Surya Prakash R, Sinha A, Tomar G, Ravikrishna RV (2018) Liquid jet in crossflow—effect of liquid entry conditions. Exp Therm Fluid Sci 93:45–56

Wang F, Fang T (2015) Liquid jet breakup for non-circular orifices under low pressures. Int J Multiph Flow 72:248–262

Wang XH, Huang Y, Wang SL, Liu ZL (2012) Bag breakup of turbulent liquid jets in crossflows. AIAA J 50(6):1360–1366

Wu PK, Kirkendall KA, Fuller RP, Nejad AS (1997) Breakup processes of liquid jets in subsonic crossflows. J Propuls Power 13(1):64–72

Wu L, Wang Z, Li Q, Li C (2016) Study on transient structure characteristics of round liquid jet in supersonic crossflows. J Vis 19:337–341

Xiao F, Dianat M, McGuirk JJ (2013) Large eddy simulation of liquid-jet primary breakup in air crossflow. AIAA J 51:2878–2893

Yu S, Yin B, Deng W, Jia H, Ye Z, Xu B, Xu H (2018) Internal flow and spray characteristics for elliptical orifice with large aspect ratio under typical diesel engine operation conditions. Fuel 228:62–73